Non-Orthogonal Multiple Access with Improper Gaussian Signaling

H. D. Tuan, A. A. Nasir, H. H. Nguyen, T. Q. Duong and H. V. Poor

***Abstract*—Improper Gaussian signaling (IGS) helps to improve the throughput of a wireless communication network by taking advantage of the additional degrees of freedom in signal processing at the transmitter. This paper exploits IGS in a general multiuser multi-cell network, which is subject to both intra-cell and inter-cell interference. With IGS under orthogonal multiple access (OMA) or non-orthogonal multiple access (NOMA), designs of transmit beamforming to maximize the users' minimum throughput subject to transmit power constraints are addressed. Such designs are mathematically formulated as nonconvex optimization problems of structured matrix variables, which cannot be solved by popular techniques such as weighted minimum mean square error or convex relaxation. By exploiting the lowest computational complexity of 2×2 linear matrix inequalities, lower concave approximations are developed for throughput functions, which are the main ingredients for devising efficient algorithms for finding solution of these difficult optimization problems. Numerical results obtained under practical scenarios reveal that (i) there is an almost two-fold gain in the throughput by employing IGS instead of the conventional proper Gaussian signaling (PGS) under both OMA and NOMA; and (ii) NOMA-IGS offers better throughput compared to that achieved by OMA-IGS.**

***Index Terms*—Transmission beamforming, improper Gaussian signaling (IGS), non-orthogonal multiple access (NOMA), multi-cell networks, nonconvex optimization, 2×2 linear matrix inequality**

This work was supported in part by Institute for Computational Science and Technology, Hochiminh city, Vietnam, in part by the Australian Research Councils Discovery Projects under Project DP190102501, in part by the KFUPM Research Project #SB171005, in part by Natural Sciences and Engineering Research Council of Canada (NSERC) under Project RGPIN-2017-05899, in part by the U.K. Royal Academy of Engineering Research Fellowship under Grant RF1415\14\22, in part by U.S. National Science Foundation under Grants CCF-093970 and CCF-1513915, and in part by Vietnam National Foundation for Science and Technology Development (NAFOSTED) under Grant No. 102.04-2017.301

Hoang D. Tuan is with the School of Electrical and Data Engineering, University of Technology Sydney, Broadway, NSW 2007, Australia (e-mail: tuan.hoang@uts.edu.au).

Ali A. Nasir is with the Department of Electrical Engineering, King Fahd University of Petroleum and Minerals (KFUPM), Dhahran, Saudi Arabia (e-mail: anasir@kfupm.edu.sa).

Ha H. Nguyen is with the Department of Electrical and Computer Engineering, University of Saskatchewan, Saskatoon, SK, Canada (e-mail: ha.nguyen@usask.ca).

Trung Q. Duong is with Queen's University Belfast, Belfast BT7 1NN, UK (email: trung.q.duong@qub.ac.uk)

H. Vincent Poor is with the Department of Electrical Engineering, Princeton University, Princeton, NJ 08544, USA (e-mail: poor@princeton.edu).

I. Introduction

The pressing need for wireless spectrum sharing among users offers the opportunities for applications of signal processing techniques at both transmit and receive ends to manage not only the background noise but also diversified interference sources such as intra-cell and inter-cell interference. Conventionally, communication systems use proper Gaussian signaling (PGS), under which transmit signals are proper Gaussian, so they are uncorrelated with their complex conjugates and their probability distribution is invariant under rotation in the complex plane. As such, they are fully characterized by their covariance matrix and can be generated from proper Gaussian information bearing sources by linear precoding. Using PGS thus simplifies the task of analyzing the performance of communication systems. Moreover, for Gaussian noise-limited channels such as single-user channels, conventional PGS is optimal [1]. In terms of sum-capacity, PGS is also optimal for multiple-input single-output (MISO) and multiple-input multiple-output (MIMO) broadcast channels by dirty-paper-coding (DPC) [2]–[5]. As clearly explained in [6], with DPC, there is one user who does not suffer any interference so the optimal transmit signal for this user is proper complex Gaussian as in the single-user case. The next user is interfered with the previous user only, whose signal is already proper complex Gaussian, so the optimal transmit signal of the next user is also proper complex Gaussian. The reasoning can be successively applied to all users. An important observation is that the optimality of PGS is strictly tied to DPC, which is not practical for more than two users.

In contrast to PGS, improper Gaussian signaling (IGS) relaxes the Gaussian properness to attain additional degrees of signaling freedom. The improperness of the transmit signals in IGS implies that they are correlated with their complex conjugates, making their pseudo-covariance matrix nonzero. As such, they must be generated from proper Gaussian information bearing sources by widely linear precoding. The superiority of IGS over PGS in terms of degree of freedom has been analyzed in single-input single-output (SISO) interference channel [7]–[13], MIMO interference channel [14]–[19], where there are multiple unicast transmitter-receiver pairs to share the spectrum medium over the same time. The achieved degree of freedom by IGS in broadcast communications has also been analysed

in [15], [20].[1]

As the joint design of IGS covariance and pseudo-covariance matrices in MISO broadcast channel is highly complex, [21] addressed their design separately by semi-definite relaxation (SDR), which is computationally inefficient as it involves matrix optimization of augmented dimensionality [22], [23]. In addition, since rank-one constraint is dropped, SDR may fail to find just a feasible point, especially, when there are many constraints or the objective function is non-smooth (such as a max-min function). The additional SDR-based randomization for locating a feasible point is both theoretically and practically inefficient [22].

On the other hand, non-orthogonal multiple access (NOMA) [24]–[26], which allows some users to access channels of other users in such a way that interference is reduced, is one of the promising strategies to accommodate more users in sharing spectrum as compared to the conventional orthogonal multiple access (OMA) [27], [28]. Naturally, PGS for OMA (PGS-OMA) and for NOMA (PGS-NOMA) have been comprehensively studied in multi-cell broadcast interference networks (see e.g. [23], [29]–[32] and references therein). In particular, based on a nonsmooth (non-differentiable) function optimization model proposed firstly in [29], references [31], [32] show that the design problem of PGS-NOMA is not more computationally difficult than that of PGS-OMA. In fact, both problems can be efficiently solved by path-following computational procedures, which are based on the same nonconcave function approximation framework.

Against the above background, the present paper aims to lay down the nonconvex optimization foundation for designing IGS for both OMA (OMA-IGS) and NOMA (NOMA-IGS) in a general multi-cell broadcast communication network, where the multi-antenna base station (BS) in each cell serves multiple single-antenna users. To the authors' best knowledge, this is the first paper to consider NOMA-IGS. The problem of designing IGS is fundamentally different from that of PGS because the latter is based on logarithmic function optimization in beamforming vectors while the former is based on log-determinant function optimizations in structured matrix variables of beamforming vectors. The universal convex quadratic optimization based approach in [30], [31] for MIMO optimization is still applicable to these complex optimization problems of IGS. However, this paper develops a much more efficient optimization technique for their computation, which is based on linear matrix inequality (LMI) optimization.

Since the pioneering work in [33], which formulates the reduced-order $\mathcal{H}_\infty$ control synthesis for linear time-invariant systems as a rank-constrained LMI optimization problem in Lyapunov matrix variables, LMI optimization became the irreplaceable tool in augmenting the power of convex optimization in solving nonconvex control problems (see, e.g. [34] and [35] and references therein). LMI optimization is often more computationally complex than convex quadratic optimization [36]. However, the LMI obtained in this paper is of the lowest size, namely 2×2, so its computational complexity is the same as that of convex quadratic programming while it provides a better approximation mean since it maximally exploits partial convex structures of the problems.[2] To summarize, our work is novel and contributive in the following aspects:

- We develop a new universal lower concave approximation for multi-output throughput functions, which are log-determinant functions in IGS beamforming vectors. Accordingly, we propose path-following algorithms to obtain solutions of both OMA-IGS and NOMA-IGS problems, which invoke $2\times$ LMI optimization of the lowest-computational complexity at each iteration and rapidly converge at least to a locally optimal solution.
- The computational efficiency of the developed algorithms allows us to simulate and analyze the performance of OMA-IGS and NOMA-IGS under both single-cell and multi-cell setups. The rigorously-conducted tests by varying different sets of simulation parameters, e.g., number of BS antennas, number of users, BS transmit power, or noise power reveal that there is almost two-fold gain in the throughput by employing IGS instead of PGS under both NOMA and OMA systems. Furthermore, with IGS, NOMA offers better throughput compared to that achieved by OMA.

The rest of the paper is organized as follows. Section II is devoted to studying OMA-IGS. In particular, a new lower concave approximation for the log-determinant function of improper Gaussian signaling throughput is developed in this section. Section III is devoted to the study of NOMA-IGS, which makes use of the function approximation developed in Section II. Section IV provides comprehensive numerical results to substantiate the theoretical results established in Sections II and III. Finally, Section V concludes the paper.

Notation. Bold-faced upper-case letters, e.g., $\mathbf{X}$ are used for matrices, bold-faced lower-case letters, e.g., $\mathbf{x}$, are used for vectors, and normal lower-case letters, e.g., x, are used for for scalars. $\mathbf{I}_n$ is the identity matrix of size $n \times n$. $\mathbf{X}^H$, $\mathbf{X}^T$, and $\mathbf{X}^*$ are the Hermitian transpose, normal transpose, and conjugate of the matrix $\mathbf{X}$, respectively. The inner product $\langle \mathbf{X}, \mathbf{Y} \rangle$ of the matrices $\mathbf{X}$ and $\mathbf{Y}$ is defined as trace$(\mathbf{X}^H\mathbf{Y})$. Denote by $\langle \mathbf{X} \rangle$ the trace of the matrix $\mathbf{X}$, and by $|\mathbf{X}|$ its determinant. $\| \cdot \|$ stands for matrix's Frobenius norm or vector's Euclidean norm. $\mathbb{C}$ is the set of all complex numbers and $\mathbb{R}$ is the set of all

[1]The degree of freedom is an appropriate metric only under very high signal-to-noise ratios.

[2]2×2 LMI $\begin{bmatrix} x_1 & x_2 \\ x_2 & x_3 \end{bmatrix} \succeq 0$ is seen as the set of convex quadratic constraints $x_1 \geq 0$, $x_3 \geq 0$, and $x_1 x_3 - (x_2)^2 \geq 0$.

real numbers. $\mathbf{x} \sim \mathcal{CN}(\boldsymbol{\eta}, \mathbf{Z})$ means that $\mathbf{x}$ is a complex random vector following a circular Gaussian distribution with mean $\boldsymbol{\eta}$ and covariance matrix $\mathbf{Z}$. $\nabla f(x)$ is the gradient of function $f(\cdot)$ with respect to its variable x. $\mathbf{A} \succ 0$ means that the matrix $\mathbf{A}$ is positive definite. $\mathbb{E}\{\cdot\}$ denotes the expectation operator. $[\mathbf{X}]^2 = \mathbf{X}\mathbf{X}^T$ for real valued matrix $\mathbf{X}$. $\mathsf{Row}[a_i]_{i\in\mathcal{I}}$ arranges a_i, $i \in \mathcal{I}$ in row-block. For instance $\mathsf{Row}[a_i]_{i\in\{1,2\}} = [a_1\ a_2]$.

II. IGS for Orthogonal Multiple Access (OMA)

Consider the downlink of a multiuser multi-cell wireless communication system which consists of K cells, where the BS of each cell is equipped with N_t antennas to serve N single-antenna users (also called user equipments, or UEs) within its cell. In each cell, there are $\frac{N}{2}$ cell-centered UEs, which are located close to the BS and $\frac{N}{2}$ cell-edge UEs, which are located far away from the BS and near the cell boundary. The $\frac{N}{2}$ far UEs in each cell not only experience poorer channel conditions than other $\frac{N}{2}$ near UEs, but also suffer more severe inter-cell interference from adjacent cells. Of course the case $K = 1$ corresponds to the single-cell setup, which will also be considered in Section IV together with the case of multi-cell setup $K > 1$. In this work, we assume the availability of full channel state information at the BSs and focus on the resource allocation problem. In a single-cell setup, channel information can be obtained by uplink channel estimation via the principle of time division duplexing and channel reciprocality. In a multi-cell setup, channel state information can be acquired by different means, e.g., through coordination among BSs [37].

Let $\mathcal{K} \triangleq \{1, 2, \cdots, K\}$ and $\mathcal{N} \triangleq \{1, 2, \cdots, N\}$, where N is an even integer. The n-th UE in the k-th cell is referred to as UE $(k, n) \in \mathcal{M} \triangleq \mathcal{K} \times \mathcal{N}$. The cell-centered UEs are UE (k, n), $n \in \mathcal{N}_c \triangleq \{1, \cdots, \frac{N}{2}\}$ while the cell-edge UEs are UE (k, n), $n \in \mathcal{N}_e \triangleq \{\frac{N}{2}+1, \cdots, N\}$. Thus the set of cell-centered UEs and the set of cell-edge UEs are $\mathcal{M}_c \triangleq \mathcal{K} \times \mathcal{N}_c$ and $\mathcal{M}_e \triangleq \mathcal{K} \times \mathcal{N}_e$, respectively.

Let $\mathbf{x}_{k',n'}$ be the signal that BS k' intends to transmit to its UE (k', n'). Then the transmitted signal of BS k' is $\sum_{n'=1}^{N} \mathbf{x}_{k',n'}$. The received signal at UE (k, n) is given by

$$y_{k,n} = \sum_{(k',n')\in\mathcal{M}} \mathbf{h}_{k',k,n}\mathbf{x}_{k',n'} + n_{k,n}, \tag{1}$$

where $\mathbf{h}_{k',k,n} \in \mathbb{C}^{1\times N_t}$ is the MISO channel from BS $k' \in \mathcal{K}$ to UE (k, n), and $n_{k,n} \sim \mathcal{CN}(0, \sigma^2)$ is the background noise.

Let the message intended for UE (k', n') be $s_{k',n'} \sim \mathcal{CN}(0, 1)$. This message is processed by a widely linear precoder to produce the following IGS message for transmission:

$$\mathbf{x}_{k',n'} = \boldsymbol{w}_{1,k',n'}s_{k',n'} + \boldsymbol{w}_{2,k',n'}s^*_{k',n'}, \tag{2}$$

where $\boldsymbol{w}_{1,k',n'} \in \mathbb{C}^{N_t\times 1}$ and $\boldsymbol{w}_{2,k',n'} \in \mathbb{C}^{N_t\times 1}$. Then, the received signal in (1) at UE (k, n) is rewritten as

$$y_{k,n} = \sum_{(k',n')\in\mathcal{M}} \mathbf{h}_{k',k,n}(\boldsymbol{w}_{1,k',n'}s_{k',n'} + \boldsymbol{w}_{2,k',n'}s^*_{k',n'}) + n_{k,n}. \tag{3}$$

In what follows we use the following notations:

$$\begin{gathered}\boldsymbol{w}_{k,n} \triangleq \{\Re\{\boldsymbol{w}_{i,k,n}\}, \Im\{\boldsymbol{w}_{i,k,n}\}, i = 1, 2\} \in \mathbb{R}^{4N_t},\\ \boldsymbol{w} \triangleq \{\boldsymbol{w}_{k,n}, (k, n) \in \mathcal{M}\} \in \mathbb{R}^{4N_tKN},\\ \bar{\mathbf{H}}_{k',k,n} \triangleq \begin{bmatrix}\Re\{\mathbf{h}_{k',k,n}\} & -\Im\{\mathbf{h}_{k',k,n}\}\\ \Im\{\mathbf{h}_{k',k,n}\} & \Re\{\mathbf{h}_{k',k,n}\}\end{bmatrix} \in \mathbb{R}^{2\times(2N_t)},\end{gathered} \tag{4}$$

and

$$\begin{gathered}\bar{\mathbf{y}}_{k,n} \triangleq \begin{bmatrix}\Re\{y_{k,n}\}\\ \Im\{y_{k,n}\}\end{bmatrix} \in \mathbb{R}^2, \bar{\mathbf{s}}_{k,n} \triangleq \begin{bmatrix}\Re\{s_{k,n}\}\\ \Im\{s_{k,n}\}\end{bmatrix} \in \mathbb{R}^2,\\ \bar{\mathbf{n}}_{k,n} \triangleq \begin{bmatrix}\Re\{n_{k,n}\}\\ \Im\{n_{k,n}\}\end{bmatrix} \in \mathbb{R}^2.\end{gathered} \tag{5}$$

Also, define a linear mapping from $\mathbb{R}^{4N_t}$ to $\mathbb{R}^{(2N_t)\times 2}$:

$$\mathcal{L}(\boldsymbol{w}_{k,n}) = \begin{bmatrix}\Re\{\boldsymbol{w}_{1,k,n}\} + \Re\{\boldsymbol{w}_{2,k,n}\} & -\Im\{\boldsymbol{w}_{1,k,n}\} - \Im\{\boldsymbol{w}_{2,k,n}\}\\ \Im\{\boldsymbol{w}_{1,k,n}\} + \Im\{\boldsymbol{w}_{2,k,n}\} & \Re\{\boldsymbol{w}_{1,k,n}\} - \Re\{\boldsymbol{w}_{2,k,n}\}\end{bmatrix} \in \mathbb{R}^{(2N_t)\times 2}.$$

Then Equation (3) can be rewritten as

$$\bar{\mathbf{y}}_{k,n} = \sum_{(k',n')\in\mathcal{M}} \bar{\mathbf{H}}_{k',k,n}\mathcal{L}(\boldsymbol{w}_{k',n'})\bar{\mathbf{s}}_{k',n'} + \bar{\mathbf{n}}_{k,n}. \tag{6}$$

It is simple to verify that

$$\mathbb{E}\{[\bar{\mathbf{s}}_{k',n'}]^2\} = \frac{1}{2}\mathbf{I}_2, \mathbb{E}\{[\bar{\mathbf{n}}_{k,n}]^2\} = \frac{1}{2}\sigma^2\mathbf{I}_2, \tag{7}$$

and

$$\mathbb{E}\{[\bar{\mathbf{H}}_{k',k,n}\mathcal{L}(\boldsymbol{w}_{k',n'})\bar{\mathbf{s}}_{k',n'}]^2\} = \frac{1}{2}[\bar{\mathbf{H}}_{k',k,n}\mathcal{L}(\boldsymbol{w}_{k',n'})]^2. \tag{8}$$

Thus, the throughput at UE (k, n) in nats/sec/Hz is given by [1]

$$\rho_{k,n}(\boldsymbol{w}) = \frac{1}{2}\ln\left|\mathbf{I}_2 + \mathbb{E}\{[\bar{\mathbf{H}}_{k,k,n}\mathcal{L}(\boldsymbol{w}_{k,n})\bar{\mathbf{s}}_{k,n}]^2\} \times\left(\sum_{(k',n')\in\mathcal{M}\setminus\{(k,n)\}} \mathbb{E}\{[\bar{\mathbf{H}}_{k',k,n}\mathcal{L}(\boldsymbol{w}_{k',n'})\bar{\mathbf{s}}_{k',n'}]^2\}\right)^{-1}\right| =$$

$$\frac{1}{2}\ln\left|\mathbf{I}_2 + [\bar{\mathbf{H}}_{k,k,n}\mathcal{L}(\boldsymbol{w}_{k,n})]^2\left([\Lambda_{k,n}(\boldsymbol{w})]^2 + \sigma^2\mathbf{I}_2\right)^{-1}\right|, \tag{9}$$

where

$$\Lambda_{k,n}(\boldsymbol{w}) \triangleq \mathsf{Row}[\bar{\mathbf{H}}_{k',k,n}\mathcal{L}(\boldsymbol{w}_{k',n'})]_{(k',n')\in\mathcal{M}\setminus\{(k,n)\}}, \tag{10}$$

which is a linear mapping. For later use, we also define

$$\hat{\Lambda}_{k,n}(\boldsymbol{w}) \triangleq \mathsf{Row}[\bar{\mathbf{H}}_{k',k,n}\mathcal{L}(\boldsymbol{w}_{k',n'})]_{(k',n')\in\mathcal{M}}. \tag{11}$$

By maximizing the worst user throughput, the max-min throughput criterion ensures fairness among all users. Such a performance criterion is very common in the literature and also adopted in this paper. The max-min throughput optimization problem is formulated as:

$$\max_{\boldsymbol{w}} \ \Psi(\boldsymbol{w}) \triangleq \min_{(k,n)\in\mathcal{M}} \ \rho_{k,n}(\boldsymbol{w}) \tag{12a}$$

$$\text{s.t.} \quad \sum_{(k,n)\in\mathcal{M}} ||\boldsymbol{w}_{k,n}||^2 \leq P_k^{\max}, \ k \in \mathcal{K}. \tag{12b}$$

The objective function (12a) is not only nonconcave but also nonsmooth, making (12) very computationally difficult. Moreover, the presence of linear mappings $\mathcal{L}(\boldsymbol{w}_{k,n})$ and $\Lambda_{k,n}(\boldsymbol{w})$ in the definition (9) for the throughput function $\rho_{k,n}$ makes (12) complex structured, preventing application of the popular weighted minimum mean square error (WMMSE)-based approach [38]. This is also true even for the easier problems of smooth optimization such as the following sum throughput optimization problem

$$\max_{\boldsymbol{w}} \sum_{(k,n)\in\mathcal{M}} \rho_{k,n}(\boldsymbol{w}) \quad \text{s.t.} \quad (12b). \tag{13}$$

On the other hand, using Shur's complement to expand the determinant of 2×2 matrix in (9) as done in [21] results in even much more complex forms of the throughput functions.

Fortunately, it has been recently shown in [30], [31] that many partial convex structures of throughput functions like the function $\rho_{k,n}$ in (12) can be systematically exploited for tractable computation. Specifically, by observing that $\rho_{k,n}$ in (12) is composed from a nonlinear function f defined by

$$f(\mathbf{X}_1, \mathbf{X}_2) = \ln |\mathbf{I}_2 + [\mathbf{X}_1]^2 \left([\mathbf{X}_2]^2 + \sigma^2\mathbf{I}_2\right)^{-1}| \tag{14}$$

and linear mappings $\mathbf{X}_1(\boldsymbol{w}) \triangleq \bar{\mathbf{H}}_{k,k,n}\mathcal{L}(\boldsymbol{w}_{k,n})$ and $\mathbf{X}_2(\boldsymbol{w}) = \Lambda_{k,n}(\boldsymbol{w})$, i.e.,

$$\rho_{k,n}(\boldsymbol{w}) = f(\mathbf{X}_1(\boldsymbol{w}), \mathbf{X}_2(\boldsymbol{w})),$$

one can simply approximate $\rho_{k,n}(\boldsymbol{w})$ by approximating the function $f(\mathbf{X}_1, \mathbf{X}_2)$. Indeed, if $\tilde{f}(\mathbf{X}_1, \mathbf{X}_2)$ is a convex/concave approximation of $f(\mathbf{X}_1, \mathbf{X}_2)$ then the composed function $\tilde{f}(\mathbf{X}_1(\boldsymbol{w}), \mathbf{X}_2(\boldsymbol{w}))$ is also a convex/concave approximation of $\rho_{k,n}(\boldsymbol{w})$ because such partial convex structures are preserved under linear mappings $\mathbf{X}_1(\boldsymbol{w})$ and $\mathbf{X}_2(\boldsymbol{w})$ [39]. The key ingredient is the following result, whose proof given in the Appendix.

Lemma 1: For all matrices $\mathbf{X}_i \in \mathbb{R}^{2\times m}$ and $\bar{\mathbf{X}}_i \in \mathbb{R}^{2\times m}$, $i = 1, 2$, the following inequality holds true

$$\begin{aligned} f(\mathbf{X}_1, \mathbf{X}_2) \quad \geq \\ f(\bar{\mathbf{X}}_1, \bar{\mathbf{X}}_2) + 4 - \sigma^2\langle\left([\bar{\mathbf{X}}_2]^2 + \sigma^2\mathbf{I}_2\right)^{-1}\rangle \\ - \left\langle \sum_{i=1}^{2}[\bar{\mathbf{X}}_i]^2 + \sigma^2\mathbf{I}_2, \left(\sum_{i=1}^{2}(\bar{\mathbf{X}}_i\mathbf{X}_i^T + \mathbf{X}_i\bar{\mathbf{X}}_i^T \right.\right. \\ \left.\left. - \ [\bar{\mathbf{X}}_i]^2) + \sigma^2\mathbf{I}_2\right)^{-1}\right\rangle \\ -\langle\left([\bar{\mathbf{X}}_2]^2 + \sigma^2\mathbf{I}_2\right)^{-1}, [\mathbf{X}_2]^2\rangle, \end{aligned} \tag{15}$$

over the convex trust region constrained by the 2×2 LMI

$$\sum_{i=1}^{2}(\bar{\mathbf{X}}_i\mathbf{X}_i^T + \mathbf{X}_i\bar{\mathbf{X}}_i^T - [\bar{\mathbf{X}}_i]^2) \succeq 0. \tag{16}$$

The right hand side (RHS) of (15) is a concave function of $(\mathbf{X}_1, \mathbf{X}_2)$,[3] which matches with f at $(\bar{\mathbf{X}}_1, \bar{\mathbf{X}}_2)$. □

It is pointed out that the following inequality was obtained in [30], [31]:

$$\begin{aligned} f(\mathbf{X}_1, \mathbf{X}_2) \quad \geq \\ a + \left(2\langle\mathcal{A}, \bar{\mathbf{X}}_1\mathbf{X}_1^T\rangle - \langle\mathcal{B}, [\mathbf{X}_1]^2\rangle\right) - \langle\mathcal{B}, [\mathbf{X}_2]^2\rangle, \end{aligned} \tag{17}$$

over the polytopic trust region constrained by the linear constraint

$$2\langle\mathcal{A}, \bar{\mathbf{X}}_1\mathbf{X}_1^T\rangle - \sigma^2\langle\mathcal{B}\rangle > 0, \tag{18}$$

with $a = f(\bar{\mathbf{X}}_1, \bar{\mathbf{X}}_2) - \langle[\bar{\mathbf{X}}_1]^2, \left([\bar{\mathbf{X}}_2]^2 + \sigma^2\mathbf{I}_2\right)^{-1}\rangle - \sigma^2\langle\mathcal{B}\rangle$, $\mathcal{A} = \left([\bar{\mathbf{X}}_2]^2 + \sigma^2\mathbf{I}_2\right)^{-1}$, and $0 \preceq \mathcal{B} = \left([\bar{\mathbf{X}}_2]^2 + \sigma^2\mathbf{I}_2\right)^{-1} - \left([\bar{\mathbf{X}}_1]^2 + [\bar{\mathbf{X}}_2]^2 + \sigma^2\mathbf{I}_2\right)^{-1}$. The RHS of (17) is thus a sum of two uncorrelated concave quadratic functions $f_i(\mathbf{X}_i)$ of $\mathbf{X}_i$ over the trust region (18) for the variable $\mathbf{X}_1$ only. In contrast, the variables $\mathbf{X}_1$ and $\mathbf{X}_2$ are correlated in the RHS of (15) over the trust region (16) involving both of them. This makes the RHS of (15) more refined than the RHS of (18) for approximating the function f.

Let $\boldsymbol{w}^{(\kappa)} \triangleq \{\boldsymbol{w}_{k,n}^{(\kappa)}, (k,n) \in \mathcal{M}\}$ be a feasible point for (12) that is found at the $(\kappa-1)$th iteration. With regard to the function $\rho_{k,n}(\boldsymbol{w})$ in (12a), applying the inequality (15) for

$$\mathbf{X}_1 = \bar{\mathbf{H}}_{k,k,n}\mathcal{L}(\boldsymbol{w}_{k,n}), \ \mathbf{X}_2 = \Lambda_{k,n}(\boldsymbol{w}),$$

and

$$\bar{\mathbf{X}}_1 = \bar{\mathbf{H}}_{k,k,n}\bar{\boldsymbol{w}}_{k,n}^{(\kappa)}, \bar{\mathbf{X}}_2 = \Lambda_{k,n}(\boldsymbol{w}^{(\kappa)}),$$

yields the following lower concave approximation:

$$\begin{aligned} \rho_{k,n}(\boldsymbol{w}) \quad \geq \\ \frac{1}{2}\left(a_{k,n}^{(\kappa)} - \left\langle\mathcal{A}_{k,n}^{(\kappa)}, \left(\hat{\Lambda}_{k,n}(\boldsymbol{w})\hat{\Lambda}^T(\boldsymbol{w}^{(\kappa)}) \right.\right.\right. \\ \left.\left.\left. + \hat{\Lambda}_{k,n}(\boldsymbol{w}^{(\kappa)})\hat{\Lambda}_{k,n}^T(\boldsymbol{w}) - [\hat{\Lambda}_{k,n}(\boldsymbol{w}^{(\kappa)})]^2 + \sigma^2\mathbf{I}_2\right)^{-1}\right\rangle \\ \left. - \left\langle\mathcal{B}_{k,n}^{(\kappa)}, [\Lambda_{k,n}(\boldsymbol{w})]^2\right\rangle\right) \quad \triangleq \\ \rho_{k,n}^{(\kappa)}(\boldsymbol{w}) \end{aligned} \tag{19}$$

over the trust region

$$\begin{aligned} \hat{\Lambda}_{k,n}(\boldsymbol{w})\hat{\Lambda}^T(\boldsymbol{w}^{(\kappa)}) + \hat{\Lambda}_{k,n}(\boldsymbol{w}^{(\kappa)})\hat{\Lambda}_{k,n}^T(\boldsymbol{w}) \\ -[\hat{\Lambda}_{k,n}(\boldsymbol{w}^{(\kappa)})]^2 \succeq 0, \\ (k,n) \in \mathcal{M}, \end{aligned} \tag{20}$$

[3] $\langle\mathbf{A}, \mathbf{X}^{-1}\rangle$ with $\mathbf{A} \succeq 0$ is convex in $\mathbf{X} \succ 0$ (see e.g. [40, p. 467] or [41, Appendix A]) so the second term in the RHS of (15) is a convex function, while the third term in the RHS of (15) is obviously a concave quadratic function.

Algorithm 1 OMA-IGS Max-min Rate Optimization Algorithm

Initialization: Set $\kappa := 0$ and a feasible point $\boldsymbol{w}^{(0)}$ satisfying the power constraint (12b).

1: **repeat**
2: Solve the convex optimization problem (22) to obtain the optimal solution $\boldsymbol{w}^{(\kappa+1)}$.
3: Set $\kappa := \kappa + 1$.
4: **until** Convergence of the objective in (12).

with

$$a_{k,n}^{(\kappa)} \triangleq 2\rho_{k,n}(\boldsymbol{w}^{(\kappa)}) + 4 - \sigma^2 \left\langle \left([\Lambda_{k,n}(\boldsymbol{w}^{(\kappa)})]^2 + \sigma^2 \mathbf{I}_2 \right)^{-1} \right\rangle, \quad (21a)$$

$$0 \prec \mathcal{A}_{k,n}^{(\kappa)} \triangleq [\hat{\Lambda}_{k,n}(\boldsymbol{w}^{(\kappa)})]^2 + \sigma^2 \mathbf{I}_2, \quad (21b)$$

$$0 \prec \mathcal{B}_{k,n}^{(\kappa)} \triangleq \left([\Lambda_{k,n}(\boldsymbol{w}^{(\kappa)})]^2 + \sigma^2 \mathbf{I}_2 \right)^{-1}. \quad (21c)$$

Thus, at the κ-th iteration, we solve the following convex optimization problem to generate the next iterative feasible point $\boldsymbol{w}^{(\kappa+1)}$ for (12):

$$\max_{\boldsymbol{w}} \ \Psi^{(\kappa)}(\boldsymbol{w}) \triangleq \min_{(k,n)\in\mathcal{M}} \ \rho_{k,n}^{(\kappa)}(\boldsymbol{w}) \quad \text{s.t.} \quad (12b), (20). \quad (22)$$

This problem involves $2KNN_t$ decision variables and K quadratic constraints in (12b) of power constraint plus KN 2×2 LMI constraints (20) of trust region, so its computational complexity is $\mathcal{O}\left((2KNN_t)^3 (KN + K)\right)$ [36, p. 4].

Algorithm 1 outlines the steps to solve the the max-min rate problem (12). Note that

$$\Psi_{k,n}^{(\kappa)}(\boldsymbol{w}^{(\kappa+1)}) > \Psi_{k,n}^{(\kappa)}(\boldsymbol{w}^{(\kappa)})$$

because $\boldsymbol{w}^{(\kappa+1)}$ is the optimal solution of (22) while $\boldsymbol{w}^{(\kappa)}$ is its feasible point. Therefore,

$$\begin{aligned} \Psi(\boldsymbol{w}^{(\kappa+1)}) &\geq \Psi^{(\kappa)}(\boldsymbol{w}^{(\kappa+1)}) \\ &> \Psi^{(\kappa)}(\boldsymbol{w}^{(\kappa)}) \\ &= \Psi(\boldsymbol{w}^{(\kappa)}), \end{aligned} \quad (23)$$

where the last equality follows from the equality $\rho_{k,n}^{(\kappa)}(\boldsymbol{w}^{(\kappa)}) = \rho_{k,n}(\boldsymbol{w}^{(\kappa)})$, which is easily checked using the definition (19). Algorithm 1 thus generates a sequence $\{\boldsymbol{w}^{(\kappa)}\}$ of improved feasible points for (12). Using similar arguments as in [23], it can be easily shown that Algorithm 1 at least converges to a locally optimal solution of (12), which satisfies the Karush-Kuh-Tucker (KKT) optimality condition. It is noteworthy to point out that the simulation results in [23] show that this type of solution is often globally optimal.

Before closing this section, let us mention that the following problem of sum throughput maximization subject to quality-of-service (QoS) constraints

$$\max_{\boldsymbol{w}} \sum_{(k,n)\in\mathcal{M}} \rho_{k,n}(\boldsymbol{w}) \quad \text{s.t.} \quad (12b), \ \rho_{k,n}(\boldsymbol{w}) \geq \gamma_{k,n}, (k,n) \in \mathcal{M} \quad (24)$$

can be addressed similarly, where its next iterative feasible point $\boldsymbol{w}^{(\kappa+1)}$ is generated as the optimal solution of the convex optimization problem

$$\max_{\boldsymbol{w}} \sum_{(k,n)\in\mathcal{M}} \rho_{k,n}^{(\kappa)}(\boldsymbol{w}) \quad \text{s.t.} \quad (12b), \ \rho_{k,n}^{(\kappa)}(\boldsymbol{w}) \geq \gamma_{k,n}, (k,n) \in \mathcal{M}. \quad (25)$$

Compared to the problem of sum throughput maximization (13), the problem (25) is much more meaningful as it enables the network to serve all its users by setting the QoS constraints in terms of users' throughput in (25). Without these QoS constraints, the network will concentrate its throughput at a few users of the best channel condition, offering almost zero throughput to other users.

III. IGS for Non-orthogonal multiple access (NOMA)

With NOMA, by exploiting the large difference in the channel conditions between the cell-centered and cell-edge UEs, each cell-centered UE $(k,n) \in \mathcal{N}_c$ is randomly paired with cell-edge UE $(k, p(n)) \in \mathcal{N}_e$ of the same cell to create a virtual cluster. This paring operation in NOMA would improve the network throughput. For notational convenience, the paired UE $(k, p(n))$ for UE (k,n) is chosen, such that $p(n) = n + \frac{N}{2}$.

The signal received by cell-centered UE $(k,n) \in \mathcal{M}_c$ is given by the same expression (3), while the signal received by cell-edge UE $(k, p(n)) \in \mathcal{M}_e$ can be expressed as

$$y_{k,p(n)} = \sum_{(k',n')\in\mathcal{M}} \mathbf{h}_{k',k,p(n)} (\boldsymbol{w}_{1,k',n'} s_{k',n'} + \boldsymbol{w}_{2,k',n'} s_{k',n'}^*) + n_{k,p(n)}, \quad (26)$$

which is rewritten similarly to (6) as

$$\bar{\mathbf{y}}_{k,p(n)} = \sum_{(k',n')\in\mathcal{M}} \bar{\mathbf{H}}_{k',k,p(n)} \mathcal{L}(\boldsymbol{w}_{k',n'}) \bar{\mathbf{s}}_{k',n'} + \bar{\mathbf{n}}_{k,p(n)}. \quad (27)$$

In NOMA, the information $s_{k,p(n)}$ is first decoded by both the cell-centered UE (k,n) and the cell-edge UE $(k,p(n))$. As such the throughput of UE $(k,p(n))$ is given by the minimum of the two throughput expressions, i.e.,

$$\tilde{\rho}_{k,p(n)}(\boldsymbol{w}) = \min\{\tilde{\rho}_{k,p(n)}^{(1)}(\boldsymbol{w}), \tilde{\rho}_{k,p(n)}^{(2)}(\boldsymbol{w})\}. \quad (28)$$

In particular, the term $\tilde{\rho}^{(1)}_{k,p(n)}(\boldsymbol{w})$ in (28) is the throughput at UE (k,n), when trying to decode $s_{k,p(n)}$:

$$\tilde{\rho}^{(1)}_{k,p(n)}(\boldsymbol{w}) = \frac{1}{2}\ln\left|\mathbf{I}_2+[\bar{\mathbf{H}}_{k,k,n}\mathcal{L}(\boldsymbol{w}_{k,p(n)})]^2 \times\left([\Upsilon^{(1)}_{k,p(n)}(\boldsymbol{w})]^2+\sigma^2\mathbf{I}_2\right)^{-1}\right|, \quad (29)$$

with

$$\Upsilon^{(1)}_{k,p(n)}(\boldsymbol{w}) \triangleq \mathsf{Row}[\bar{\mathbf{H}}_{k',k,n}\mathcal{L}(\boldsymbol{w}_{k',n'})]_{(k',n')\in\mathcal{M}\setminus\{(k,p(n))\}}. \quad (30)$$

Likewise, $\tilde{\rho}^{(2)}_{k,p(n)}(\boldsymbol{w})$ is the throughput at UE $(k,p(n))$, when trying to decode its own information $s_{k,p(n)}$:

$$\tilde{\rho}^{(2)}_{k,p(n)}(\boldsymbol{w}) = \frac{1}{2}\ln\left|\mathbf{I}_2+[\bar{\mathbf{H}}_{k,k,p(n)}\mathcal{L}(\boldsymbol{w}_{k,p(n)})]^2 \times\left([\Upsilon^{(2)}_{k,p(n)}(\boldsymbol{w})]^2+\sigma^2\mathbf{I}_2\right)^{-1}\right|, \quad (31)$$

with

$$\Upsilon^{(2)}_{k,p(n)}(\boldsymbol{w}) = \mathsf{Row}[\bar{\mathbf{H}}_{k',k,p(n)}\mathcal{L}(\boldsymbol{w}_{k',n'})]_{(k',n')\in\mathcal{M}\setminus\{(k,p(n))\}}. \quad (32)$$

The decoding in NOMA is such that UE $(k,n)\in\mathcal{M}_c$ first decodes the message $s_{k,p(n)}$, and then removes it from the superimposed received signal in order to decode its own information $s_{k,n}$. Thus, the throughput for decoding $s_{k,n}$ by UE (k,n) is given by

$$\tilde{\rho}_{k,n}(\boldsymbol{w}) = \frac{1}{2}\ln\left|\mathbf{I}_2+[\bar{\mathbf{H}}_{k,k,n}\mathcal{L}(\boldsymbol{w}_{k,n})]^2 \times\left([\Upsilon_{k,n}(\boldsymbol{w})]^2+\sigma^2\mathbf{I}_2\right)^{-1}\right|, \quad (33)$$

for

$$\Upsilon_{k,n}(\boldsymbol{w}) \triangleq \mathsf{Row}[\bar{\mathbf{H}}_{k',k,n}\mathcal{L}(\boldsymbol{w}_{k',n'})]_{(k',n')\in\mathcal{M}\setminus\{(k,n),(k,p(n))\}}. \quad (34)$$

The users' max-min throughput is defined by

$$\begin{aligned}\min_{(k,n)\in\mathcal{M}}\tilde{\rho}_{k,n}(\boldsymbol{w}) &= \min_{(k,n)\in\mathcal{M}_c}\min\{\tilde{\rho}_{k,n}(\boldsymbol{w}),\tilde{\rho}_{k,p(n)}(\boldsymbol{w})\} \\ &= \min_{(k,n)\in\mathcal{M}_c}\min\{\tilde{\rho}_{k,n}(\boldsymbol{w}),\min\{\tilde{\rho}^{(1)}_{k,p(n)}(\boldsymbol{w}),\tilde{\rho}^{(2)}_{k,p(n)}(\boldsymbol{w})\}\} \\ &= \min_{(k,n)\in\mathcal{M}_c}\min\{\tilde{\rho}_{k,n}(\boldsymbol{w}),\tilde{\rho}^{(1)}_{k,p(n)}(\boldsymbol{w}),\tilde{\rho}^{(2)}_{k,p(n)}(\boldsymbol{w})\}. \quad (35)\end{aligned}$$

The max-min throughput optimization problem is then formulated as:

$$\max_{\boldsymbol{w}}\ \Phi(\boldsymbol{w}) \triangleq \min_{(k,n)\in\mathcal{M}_c}\min\{\tilde{\rho}_{k,n}(\boldsymbol{w}),\tilde{\rho}^{(1)}_{k,p(n)}(\boldsymbol{w}),\tilde{\rho}^{(2)}_{k,p(n)}(\boldsymbol{w})\} \quad \text{s.t.} \quad (12b). \quad (36)$$

Since the objective function in (36) is non-concave, in what follows, we first find the lower bound concave approximations for $\tilde{\rho}_{k,n}(\boldsymbol{w})$, $\tilde{\rho}^{(1)}_{k,p(n)}(\boldsymbol{w})$, and $\tilde{\rho}^{(2)}_{k,p(n)}(\boldsymbol{w})$. Let $\boldsymbol{w}^{(\kappa)}$ be a feasible point for (36) that is found at the $(\kappa-1)$th iteration. Similarly to (19),

$$\begin{aligned}\tilde{\rho}_{k,n}(\boldsymbol{w}) &\geq \tilde{\rho}^{(\kappa)}_{k,n}(\boldsymbol{w}) \\ &\triangleq \frac{1}{2}\Big(\tilde{a}^{(\kappa)}_{k,n}-\Big\langle\tilde{\mathcal{A}}^{(\kappa)}_{k,n},\Big(\hat{\Upsilon}_{k,n}(\boldsymbol{w})(\hat{\Upsilon}_{k,n}(\boldsymbol{w}^{(\kappa)}))^T \\ &\quad+\hat{\Upsilon}_{k,n}(\boldsymbol{w}^{(\kappa)})\hat{\Upsilon}^T_{k,n}(\boldsymbol{w}) \\ &\quad-[\hat{\Upsilon}_{k,n}(\boldsymbol{w}^{(\kappa)})]^2+\sigma^2\mathbf{I}_2\Big)^{-1}\Big\rangle \\ &\quad-\Big\langle\tilde{\mathcal{B}}^{(\kappa)}_{k,n},[\Upsilon_{k,n}(\boldsymbol{w})]^2\Big\rangle\Big) \quad (37)\end{aligned}$$

over the trust region

$$\hat{\Upsilon}_{k,n}(\boldsymbol{w})(\hat{\Upsilon}_{k,n}(\boldsymbol{w}^{(\kappa)}))^T+\hat{\Upsilon}_{k,n}(\boldsymbol{w}^{(\kappa)})\hat{\Upsilon}^T_{k,n}(\boldsymbol{w}) -[\hat{\Upsilon}_{k,n}(\boldsymbol{w}^{(\kappa)})]^2\succeq 0,\ (k,n)\in\mathcal{M}_c, \quad (38)$$

with

$$\hat{\Upsilon}_{k,n}(\boldsymbol{w}) \triangleq [\bar{\mathbf{H}}_{k',k,n}\mathcal{L}(\boldsymbol{w}_{k',n'})]_{(k',n')\in\mathcal{M}\setminus\{(k,p(n))\}}, \quad (39a)$$

$$\tilde{a}^{(\kappa)}_{k,n} \triangleq 2\tilde{\rho}_{k,n}(\boldsymbol{w}^{(\kappa)})+4 -\sigma^2\left\langle\left([\Upsilon_{k,n}(\boldsymbol{w}^{(\kappa)})]^2+\sigma^2\mathbf{I}_2\right)^{-1}\right\rangle, \quad (39b)$$

$$0\prec\tilde{\mathcal{A}}^{(\kappa)}_{k,n} \triangleq [\hat{\Upsilon}_{k,n}(\boldsymbol{w}^{(\kappa)})]^2+\sigma^2\mathbf{I}_2, \quad (39c)$$

$$0\prec\tilde{\mathcal{B}}^{(\kappa)}_{k,n} \triangleq \left([\Upsilon_{k,n}(\boldsymbol{w}^{(\kappa)})]^2+\sigma^2\mathbf{I}_2\right)^{-1}. \quad (39d)$$

Furthermore,

$$\begin{aligned}\tilde{\rho}^{(1)}_{k,p(n)}(\boldsymbol{w}) &\geq \\ \tilde{\rho}^{(1,\kappa)}_{k,p(n)}(\boldsymbol{w}) &\triangleq \\ \frac{1}{2}\Big(\tilde{a}^{(1,\kappa)}_{k,p(n)}&-\Big\langle\tilde{\mathcal{A}}^{(1,\kappa)}_{k,p(n)},\Big(\hat{\Upsilon}^{(1)}_{k,p(n)}(\boldsymbol{w})(\hat{\Upsilon}^{(1)}_{k,p(n)}(\boldsymbol{w}^{(\kappa)}))^T \\ &+\hat{\Upsilon}^{(1)}_{k,p(n)}(\boldsymbol{w}^{(\kappa)})(\hat{\Upsilon}^{(1)}_{k,p(n)}(\boldsymbol{w}))^T \\ &-[\hat{\Upsilon}^{(1)}_{k,p(n)}(\boldsymbol{w}^{(\kappa)})]^2+\sigma^2\mathbf{I}_2\Big)^{-1}\Big\rangle \\ &-\Big\langle\tilde{\mathcal{B}}^{(1,\kappa)}_{k,p(n)},[\Upsilon^{(1)}_{k,p(n)}(\boldsymbol{w})]^2\Big\rangle\Big) \quad (40)\end{aligned}$$

over the trust region

$$\hat{\Upsilon}^{(1)}_{k,p(n)}(\boldsymbol{w})(\hat{\Upsilon}^{(1)}_{k,p(n)}(\boldsymbol{w}^{(\kappa)}))^T+ \hat{\Upsilon}^{(1)}_{k,p(n)}(\boldsymbol{w}^{(\kappa)})(\hat{\Upsilon}^{(1)}_{k,p(n)}(\boldsymbol{w}))^T-[\hat{\Upsilon}^{(1)}_{k,p(n)}(\boldsymbol{w}^{(\kappa)})]^2\succeq 0, \quad (41)$$
$$(k,n)\in\mathcal{M}_c,$$

with

$$\hat{\Upsilon}^{(1)}_{k,p(n)}(\boldsymbol{w}) \triangleq \mathsf{Row}[\bar{\mathbf{H}}_{k',k,n}\mathcal{L}(\boldsymbol{w}_{k',n'})]_{(k',n')\in\mathcal{M}}, \quad (42a)$$

$$\tilde{a}^{(1,\kappa)}_{k,p(n)} \triangleq 2\tilde{\rho}^{(1)}_{k,p(n)}(\boldsymbol{w}^{(\kappa)})+4 -\sigma^2\left\langle\left([\Upsilon^{(1)}_{k,p(n)}(\boldsymbol{w}^{(\kappa)})]^2+\sigma^2\mathbf{I}_2\right)^{-1}\right\rangle, \quad (42b)$$

$$0\prec\tilde{\mathcal{A}}^{(1,\kappa)}_{k,p(n)} \triangleq [\hat{\Upsilon}^{(1)}_{k,p(n)}(\boldsymbol{w}^{(\kappa)})]^2+\sigma^2\mathbf{I}_2, \quad (42c)$$

$$0\prec\tilde{\mathcal{B}}^{(1,\kappa)}_{k,p(n)} \triangleq \left([\Upsilon^{(1)}_{k,p(n)}(\boldsymbol{w}^{(\kappa)})]^2+\sigma^2\mathbf{I}_2\right)^{-1}. \quad (42d)$$

Likewise,

$$\begin{aligned}\tilde{\rho}^{(2)}_{k,p(n)}(\boldsymbol{w}) &\geq \\ \tilde{\rho}^{(2,\kappa)}_{k,p(n)}(\boldsymbol{w}) &\triangleq \\ \frac{1}{2}\Big(\tilde{a}^{(2,\kappa)}_{k,p(n)} - \Big\langle \tilde{\mathcal{A}}^{(2,\kappa)}_{k,p(n)}, \Big(\hat{\Upsilon}^{(2)}_{k,p(n)}(\boldsymbol{w})(\hat{\Upsilon}^{(2)}_{k,p(n)}(\boldsymbol{w}^{(\kappa)}))^T \\ + \hat{\Upsilon}^{(2)}_{k,p(n)}(\boldsymbol{w}^{(\kappa)})(\hat{\Upsilon}^{(2)}_{k,p(n)}(\boldsymbol{w}))^T \\ - [\hat{\Upsilon}^{(2)}_{k,p(n)}(\boldsymbol{w}^{(\kappa)})]^2 + \sigma^2\mathbf{I}_2\Big)^{-1}\rangle \\ - \Big\langle \tilde{\mathcal{B}}^{(\kappa)}_{k,p(n)}, [\Upsilon^{(2)}_{k,p(n)}(\boldsymbol{w})]^2\Big\rangle\Big) \quad (43)\end{aligned}$$

over the trust region

$$\begin{aligned}\hat{\Upsilon}^{(2)}_{k,p(n)}(\boldsymbol{w})(\hat{\Upsilon}^{(2)}_{k,p(n)}(\boldsymbol{w}^{(\kappa)}))^T + \\ \hat{\Upsilon}^{(2)}_{k,p(n)}(\boldsymbol{w}^{(\kappa)})(\hat{\Upsilon}^{(2)}_{k,p(n)}(\boldsymbol{w}))^T - [\hat{\Upsilon}^{(2)}_{k,p(n)}(\boldsymbol{w}^{(\kappa)})]^2 \succeq 0, \quad (44) \\ (k,n) \in \mathcal{M}_c,\end{aligned}$$

with

$$\hat{\Upsilon}^{(2)}_{k,p(n)}(\boldsymbol{w}) \triangleq [\bar{\mathbf{H}}_{k',k,p(n)}\mathcal{L}(\boldsymbol{w}_{k',n'})]_{(k',n')\in\mathcal{M}}, \quad (45a)$$

$$\begin{aligned}\tilde{a}^{(2,\kappa)}_{k,p(n)} \triangleq 2\tilde{\rho}^{(2)}_{k,p(n)}(\boldsymbol{w}^{(\kappa)}) + 4 \\ -\sigma^2\left\langle\left([\Upsilon^{(2)}_{k,p(n)}(\boldsymbol{w}^{(\kappa)}) + \sigma^2\mathbf{I}_2\right)^{-1}\right\rangle, \quad (45b)\end{aligned}$$

$$0 \prec \tilde{\mathcal{A}}^{(2,\kappa)}_{k,p(n)} \triangleq [\hat{\Upsilon}^{(2)}_{k,p(n)}(\boldsymbol{w}^{(\kappa)})]^2 + \sigma^2\mathbf{I}_2, \quad (45c)$$

$$0 \prec \tilde{\mathcal{B}}^{(2,\kappa)}_{k,p(n)} \triangleq \left([\Upsilon^{(2)}_{k,p(n)}(\boldsymbol{w}^{(\kappa)})]^2 + \sigma^2\mathbf{I}_2\right)^{-1}. \quad (45d)$$

Thus, at the κ-th iteration, we solve the following convex optimization problem to generate the next iterative feasible point $\boldsymbol{w}^{(\kappa+1)}$ for (36)

$$\begin{aligned}\max_{\boldsymbol{w}}\ \Phi^{(\kappa)}(\boldsymbol{w}) \triangleq \min_{(k,n)\in\mathcal{M}_c} \min\{\tilde{\rho}^{(\kappa)}_{k,n}(\boldsymbol{w}), \tilde{\rho}^{(1,\kappa)}_{k,p(n)}(\boldsymbol{w}), \\ \tilde{\rho}^{(2,\kappa)}_{k,p(n)}(\boldsymbol{w})\} \\ \text{s.t.} \quad (12b), (38), (41), (44). \quad (46)\end{aligned}$$

Compared to OMA-IGS iteration (22), this NOMA IGS iteration involves the same number $2KNN_t$ of decision variables but more $KN/2$ 2×2 LMI constraints (44), so its computational complexity is $\mathcal{O}\left((2KNN_t)^3(1.5KN+K)\right)$.

Algorithm 2 outlines the steps to solve the max-min rate problem (36). Similar to (23) one has:

$$\Phi(\boldsymbol{w}^{(\kappa+1)}) > \Phi(\boldsymbol{w}^{(\kappa)}),$$

and like Algorithm 1, it can be shown that Algorithm 2 at least converges to a locally optimal solution of (36).

Like the problem (24) for OMA, the problem of NOMA sum throughput maximization subject to QoS constraints is formulated as

$$\begin{aligned}\max_{\boldsymbol{w}} \sum_{(k,n)\in\mathcal{M}} \tilde{\rho}_{k,n}(\boldsymbol{w}) \quad \text{s.t.} \quad (12b), \\ \tilde{\rho}_{k,n}(\boldsymbol{w}) \geq \gamma_{k,n}, (k,n) \in \mathcal{M}, \quad (47)\end{aligned}$$

Algorithm 2 NOMA-IGS Max-Min Rate Optimization Algorithm

Initialization: Set $\kappa := 0$ and a feasible point $\boldsymbol{w}^{(0)}$ satisfying the power constraint (12b).

1: **repeat**
2: Solve the convex optimization problem (46) to obtain the optimal solution $\boldsymbol{w}^{(\kappa+1)}$.
3: Set $\kappa := \kappa + 1$.
4: **until** Convergence for the objective in (36).

where $\gamma_{k,n}$ is the user (k,n)'s throughput threshold. By using the expression (28) for the throughput function $\tilde{\rho}_{k,p(n)}(\boldsymbol{w})$ of user $(k,p(n)) \in \mathcal{M}_e$, we can rewrite (47) by

$$\begin{aligned}\max_{\boldsymbol{w}} \sum_{(k,n)\in\mathcal{M}_c} \Big[\tilde{\rho}_{k,n}(\boldsymbol{w}) + \min\{\tilde{\rho}^{(1)}_{k,p(n)}(\boldsymbol{w}), \\ \tilde{\rho}^{(2)}_{k,p(n)}(\boldsymbol{w})\}\Big] \quad \text{s.t.} \quad (12b), \quad (48a)\end{aligned}$$

$$\tilde{\rho}_{k,n}(\boldsymbol{w}) \geq \gamma_{k,n}, (k,n) \in \mathcal{M}_c, \quad (48b)$$

$$\begin{aligned}\min\{\tilde{\rho}^{(1)}_{k,p(n)}(\boldsymbol{w}), \tilde{\rho}^{(2)}_{k,p(n)}(\boldsymbol{w})\} \geq \gamma_{k,n(p)}, \quad (48c) \\ (k,n) \in \mathcal{M}_c,\end{aligned}$$

which can be computed by generating the next iterative feasible point $\boldsymbol{w}^{(\kappa+1)}$ as the optimal solution of the convex optimization problem

$$\begin{aligned}\sum_{(k,n)\in\mathcal{M}_c} \Big[\tilde{\rho}^{(\kappa)}_{k,n}(\boldsymbol{w}) + \min\{\tilde{\rho}^{(1,\kappa)}_{k,p(n)}(\boldsymbol{w}), \\ \tilde{\rho}^{(2,\kappa)}_{k,p(n)}(\boldsymbol{w})\}\Big] \quad \text{s.t.} \quad (12b), \quad (49a)\end{aligned}$$

$$\tilde{\rho}^{(\kappa)}_{k,n}(\boldsymbol{w}) \geq \gamma_{k,n}, (k,n) \in \mathcal{M}_c, \quad (49b)$$

$$\begin{aligned}\tilde{\rho}^{(1,\kappa)}_{k,p(n)}(\boldsymbol{w}) \geq \gamma_{k,n(p)}, \tilde{\rho}^{(2,\kappa)}_{k,p(n)}(\boldsymbol{w})\} \geq \gamma_{k,n(p)}, \quad (49c) \\ (k,n) \in \mathcal{M}_c.\end{aligned}$$

IV. Simulation Results

In all simulations, the channel $\mathbf{h}_{k',k,n}$ from BS $k' \in \mathcal{K}$ to UE (k,n) at a distance of d meters is generated as

$$\mathbf{h}_{k',k,n} = \sqrt{10^{-\sigma^2_{\text{PL}}/10}}\tilde{\mathbf{h}}_{k',k,n}.$$

In the above, $\tilde{\mathbf{h}}_{k',k,n}$ is a normalized Rayleigh fading channel gain, if $k' = k$ and $n \in \mathcal{N}_e$ (channels between the BS and its own cell-edge users), or if $k' \neq k$ (channels between the BS and users in neighboring cells). On the other hand, $\tilde{\mathbf{h}}_{k',k,n}$ is a normalized Rician fading channel with a Rician factor of 0 dB if $k' = k$ and $n \in \mathcal{N}_c$ (channels between the BS and its own cell-centered users). The path loss (in dB) is specified as

$$\sigma^2{}_{\text{PL}} = 38.46 + 10\beta\log_{10}(d),$$

where the loss factor 38.46 is the free space path loss at a reference distance of 1 meter at carrier frequency of 2 GHz [42], and β is the path-loss exponent. For the Rician

fading channels between the BS and its own cell-centered UEs ($k' = k$ and $n \in \mathcal{N}_c$), β is set to be 2, while for the Rayleigh fading channels, β is set to 3.1 [42].

For simplicity, the same power budget is set for each cell, i.e., $P_k^{\max} \equiv P^{\max}$, $\forall\ k \in \mathcal{K}$. Unless stated otherwise, $P^{\max} = 26$ dBm, and the noise power spectral density $\frac{\sigma^2}{B} = -174$ dBm/Hz with bandwidth $B = 20$ MHz. To analyze the performance of the proposed algorithms, we present simulation results separately for both single-cell ($K = 1$) and multi-cell ($K > 1$) setups. We follow [32, Algorithm 3] for evaluating the performance of the corresponding OMA-PGS and NOMA-PGS.

A. Results for a Single-Cell Network ($K = 1$)

We setup a single-cell network as shown in Fig. 1, which simulates an urban micro-cellular environment with a cell radius of 300 meters, where the cell-centered UEs are placed around the distance of 110 meters from the BS while the cell-edge users are placed at a distance of about 265 meters from the BS [42]. In this subsection, unless stated otherwise, we consider $N = 8$ UEs with four cell-centered and four cell-edge UEs and $N_t = 6$ transmit antennas at each BS.

Fig. 2 shows the convergence of the proposed algorithms (Algorithms 1 and 2) under $N_t = 6$ BS antennas, $K = 1$ cell, $N = 8$ UEs, and $P^{\max} = 26$ dBm. Fig. 2 shows that both Algorithm 2 (NOMA-IGS) and Algorithm 1 (OMA-IGS) converge after approximately within 40 iterations. The computational complexities of Algorithms 1 and 2 are given in Table I, which shows the rounded average number of iterations over different channel realizations, number of decision variables, and number of quadratic/LMI constraints.

TABLE I
COMPUTATIONAL COMPLEXITIES OF THE PROPOSED ALGORITHMS UNDER $N_t = 6$ BS ANTENNAS, $K = 1$ CELL, $N = 8$ UES, AND $P^{\max} = 26$ DBM.

Alg.	# iterations	# variables	# constraints
Alg. 1	30	96	9
Alg. 2	44	96	13

Fig. 3 plots the optimized worst user rate versus varying number of BS antennas N_t, for fixed $K = 1$ cells, $N = 8$ UEs, and $P^{\max} = 26$ dBm. As expected, the throughput increases with the increase in the number of antennas, thanks to the larger degree of freedom. It can be seen that an approximately two-fold gain in the throughput is obtained by employing IGS instead of PGS under both NOMA and OMA systems. However, the performance gain decreases with the increase in the number of BS antennas. One important observation from Fig. 3 is that Algorithm 2 (NOMA-IGS) and Algorithm 1 (OMA-IGS) have a similar performance when the number of BS antennas N_t is the same as the number of UEs N. Fig. 4 illustrates how the optimized worst user rate decreases as the noise power spectral density $\frac{\sigma^2}{B}$ increases for fixed $N_t = 6$ BS antennas, $K = 1$ cell, $N = 8$ UEs, and $P^{\max} = 26$ dBm. Fig. 4 once again shows that there is a substantial gain, approximately two-fold gain, in the throughput by employing IGS instead of PGS under both NOMA and OMA systems. This performance gain is comes from the additional degree of freedom as captured via the non-zero pseudo-covariance matrix in IGS. Both Figs. 3 and 4 clearly show that NOMA-IGS (Algorithm 2) offers the best throughput compared to all other signaling/multiple access strategies under consideration.

Fig. 5 illustrates how the optimized worst user rate increases when increasing the BS transmit power budget $P^{\max}$, for fixed $N_t = 6$ BS antennas, $K = 1$ cell, and $N = 8$ UEs per cell. Observe that the performance gap in the throughput between IGS and PGS increases with the increase in the power budget. Fig. 6 plots optimized worst user rate versus varying number of UEs N, under fixed $N_t = 6$ BS antennas, $K = 1$ cell, and $P^{\max} = 26$ dBm. As expected, the throughput decreases with the increase in the number of UEs per cell due to the increase in interference. Again, both Figs. 3 and 6 show that NOMA-IGS (Algorithm 2) offers the best throughput.

B. Results for a Multi-Cell Network ($K = 3$)

A three-cell network is depicted in Fig. 7. The radius of each cell is 300 meters, where the cell-centered UEs in each cell are placed around the distance of 110 meters from the serving BS, while the cell-edge users are placed at about 265 meters from the serving BS. In this subsection, unless stated otherwise, we consider $N = 4$ UEs with two cell-centered and two cell-edge UEs and $N_t = 3$ transmit antennas at each BS.

Fig. 8 illustrates the convergence of the proposed Algorithms 1 and 2, under $N_t = 3$ BS antennas, $K = 3$ cells, $N = 4$ UEs, and $P^{\max} = 26$ dBm. Fig. 8 shows that both Algorithm 2 (NOMA-IGS) and Algorithm 1 (OMA-IGS) converge within 25 iterations approximately. In Table II, the computational complexities of the two proposed algorithms are provided for $N_t = 3$ BS antennas, $K = 3$ cells, $N = 4$ UEs, and $P^{\max} = 26$ dBm.

TABLE II
COMPUTATIONAL COMPLEXITIES OF THE PROPOSED ALGORITHMS UNDER $N_t = 3$ BS ANTENNAS, $K = 3$ CELLS, $N = 4$ UES, AND $P^{\max} = 26$ DBM.

Alg.	# iterations	# variables	# constraints
Alg. 1	24	72	15
Alg. 2	26	72	21

Fig. 9 plots the optimized worst user rate versus varying number of BS antennas N_t, for fixed $K = 3$ cells, $N = 4$ UEs, and $P^{\max} = 26$ dBm. As in the case of single-cell setup, it can be seen that: (i) the throughput increases as the number of antennas increases, and (ii) an approximately two-fold gain in the throughput is obtained by employing

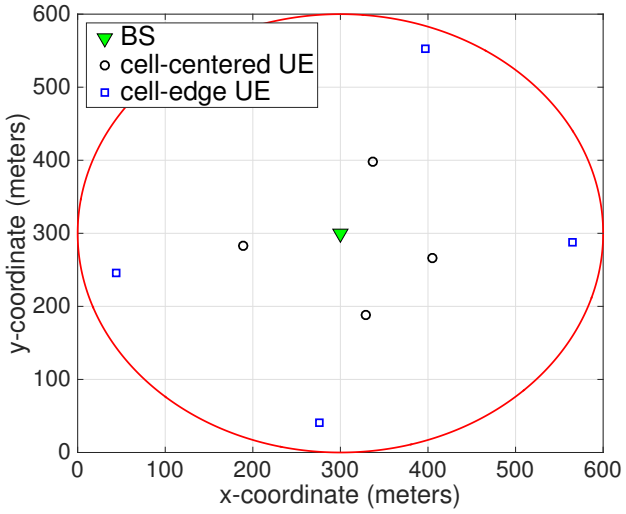

Fig. 1. A single-cell network setup.

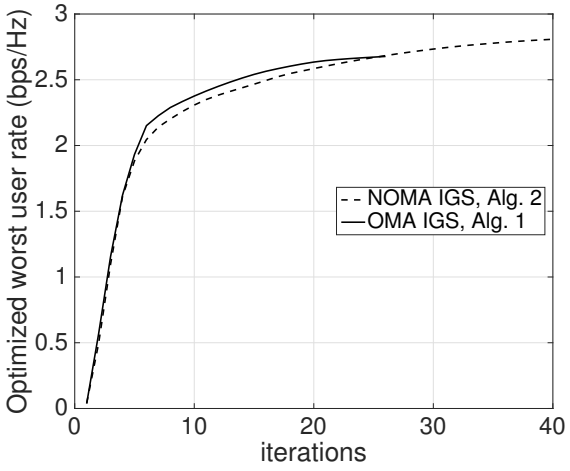

Fig. 2. Convergence of the proposed algorithms (Algorithms 1 and 2) in a single-cell setup: $N_t = 6$ BS antennas, $N = 8$ UEs, and $P^{\max} = 26$ dBm.

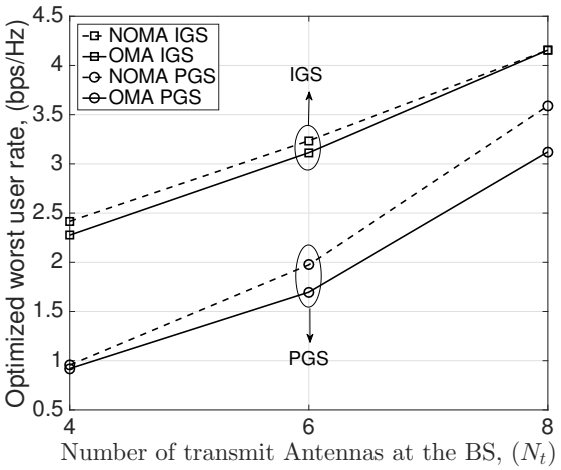

Fig. 3. Optimized worst user rate for varying number of BS antennas N_t, and fixed $K = 1$ cell, $N = 8$ UEs, $P^{\max} = 26$ dBm.

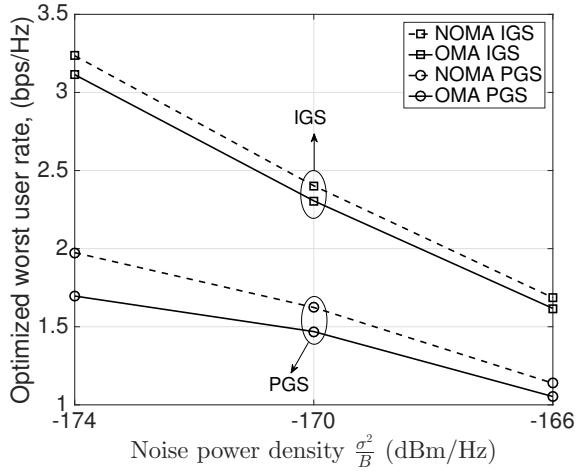

Fig. 4. Optimized worst user rate for varying values of noise power density $\frac{\sigma^2}{B}$, and fixed $N_t = 6$ BS antennas, $K = 1$ cell, $N = 8$ UEs, $P^{\max} = 26$ dBm.

IGS instead of PGS under both NOMA and OMA systems. Again, this performance gain is due to the additional degree of freedom captured via the non-zero pseudo-covariance matrix in IGS. Fig. 10 plots the optimized worst user rate versus varying number of cells K under fixed $N_t = 3$ BS antennas, $N = 4$ UEs, and $P^{\max} = 26$ dBm. As can be seen, the throughput decreases with the increase in the number of cells, which is expected since the inter-cell interference increases. We can observe from Figs. 9 and 10 that, also in a multi-cell network, NOMA-IGS offers the best throughput compared to all other alternative signaling/multiple access strategies under consideration.

V. Conclusions

This paper has considered the design problems of transmit beamforming to maximize the users' max-min throughput subject to power constraints when improper Gaussian signaling (IGS) is used in multiuser multi-cell broadcast interference networks with either orthogonal multiple access (OMA) or non-orthogonal multiple access (NOMA). The computational solution for such non-convex problems is non-trivial as the throughput functions depend on a particular structure of widely linear precoding matrices. We have developed 2×2 LMI optimization based algorithms to solve these design problems efficiently. Numerical results showed that there is almost a two-fold gain in the throughput by employing IGS instead of the conventional proper Gaussian signaling (PGS), under both OMA and NOMA. When compared with other signaling/multiple access strategies, including OMA-IGS, PGS-OMA and PGS-NOMA, it offers the best throughput.

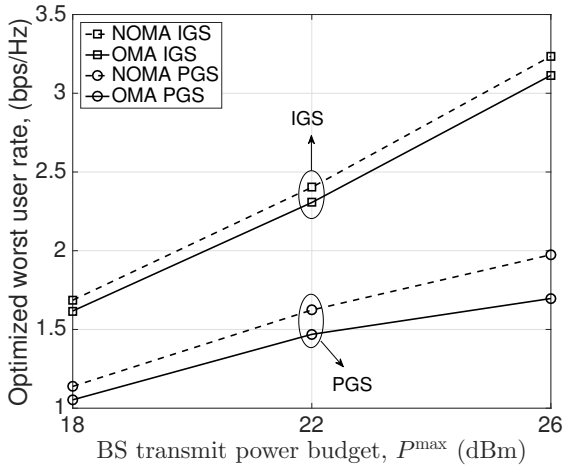

Fig. 5. Optimized worst user rate for varying values of BS transmit power budget $P^{\max}$, and fixed $N_t = 6$ BS antennas, $K = 1$ cell, $N = 8$ UEs.

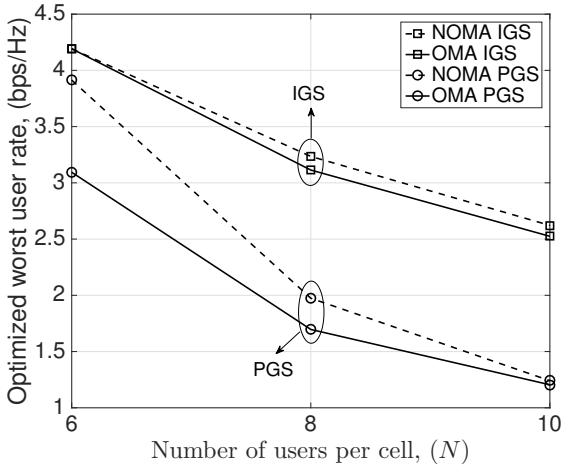

Fig. 6. Optimized worst user rate for varying number of UEs N, and fixed $N_t = 6$ BS antennas, $K = 1$ cell, $P^{\max} = 26$ dBm.

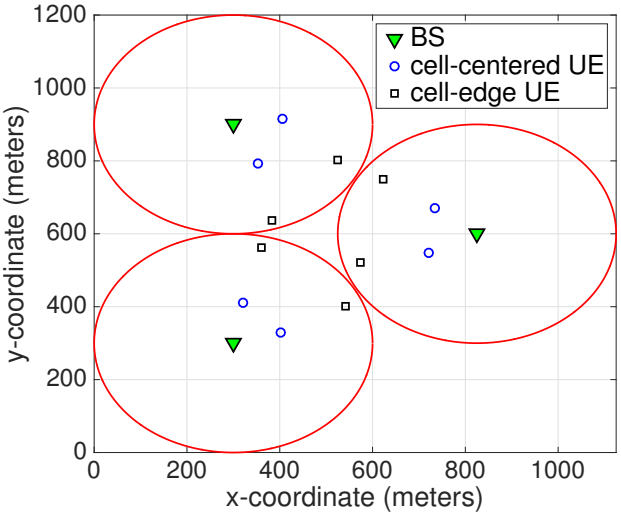

Fig. 7. A multi-cell network setup with $K = 3$ cells.

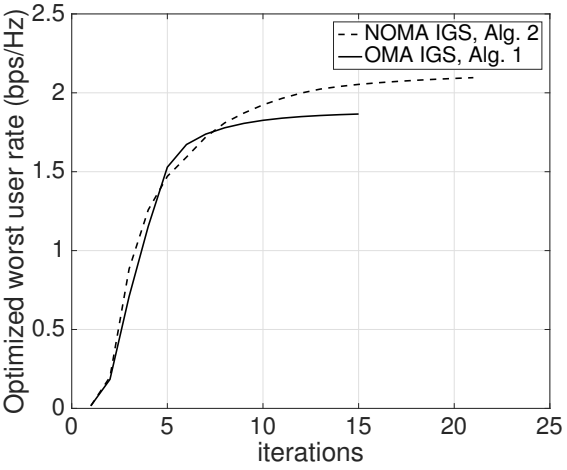

Fig. 8. Convergence of the proposed algorithms (Algorithms 1 and 2), for $N_t = 3$ BS antennas, $K = 3$ cells, $N = 4$ UEs, $P^{\max} = 26$ dBm.

APPENDIX: THE PROOF OF LEMMA 1

Since the function $\varphi(\mathbf{X}) \triangleq \ln|\mathbf{X}|$ is concave on the domain $\mathbf{X} \succ 0$, it is true that [39, Prop. 2.21, p. 62]

$$\begin{aligned} \ln|\mathbf{X}| &= \varphi(\mathbf{X}) \\ &\leq \varphi(\bar{\mathbf{X}}) + \langle \nabla\varphi(\bar{\mathbf{X}}), \mathbf{X} - \bar{\mathbf{X}} \rangle \\ &= \ln|\bar{\mathbf{X}}| - 2 + \langle \bar{\mathbf{X}}^{-1}, \mathbf{X} \rangle \end{aligned} \tag{50}$$

for all positive definite matrices $\mathbf{X}$ and $\bar{\mathbf{X}}$ of size 2×2. This also means that

$$\begin{aligned} \ln|\mathbf{X}^{-1}| &= -\varphi(\mathbf{X}) \\ &\geq \ln|\bar{\mathbf{X}}^{-1}| + 2 - \langle \bar{\mathbf{X}}^{-1}, \mathbf{X} \rangle. \end{aligned} \tag{51}$$

Making use of the fact that a matrix is positive definite if and only if its inverse is positive definite, we replace $\mathbf{X}^{-1} \to \mathbf{X}$ and $\bar{\mathbf{X}}^{-1} \to \bar{\mathbf{X}}$ in (51) to obtain

$$\ln|\mathbf{X}| \geq \ln|\bar{\mathbf{X}}| + 2 - \langle \bar{\mathbf{X}}, \mathbf{X}^{-1} \rangle, \quad \forall\, \mathbf{X} \succ 0, \bar{\mathbf{X}} \succ 0. \tag{52}$$

Now, representing the function f defined in (14) by

$$\ln|[\mathbf{X}_1]^2 + [\mathbf{X}_2]^2 + \sigma^2\mathbf{I}_2| + \ln|\left([\mathbf{X}_2]^2 + \sigma^2\mathbf{I}_2\right)^{-1}|$$

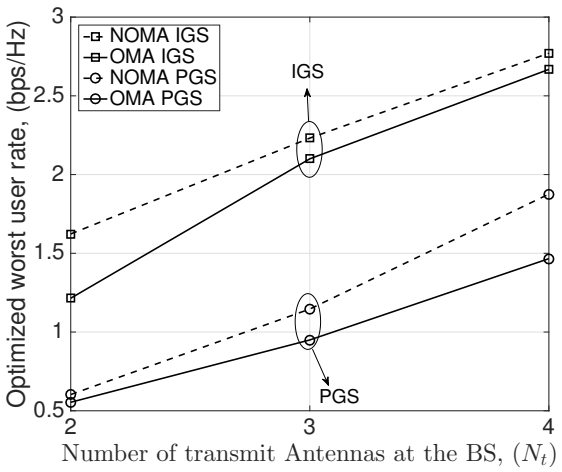

Fig. 9. Optimized worst user rate for varying number of BS antennas N_t, and fixed $K = 3$ cells, $N = 4$ UEs, and $P^{\max} = 26$ dBm.

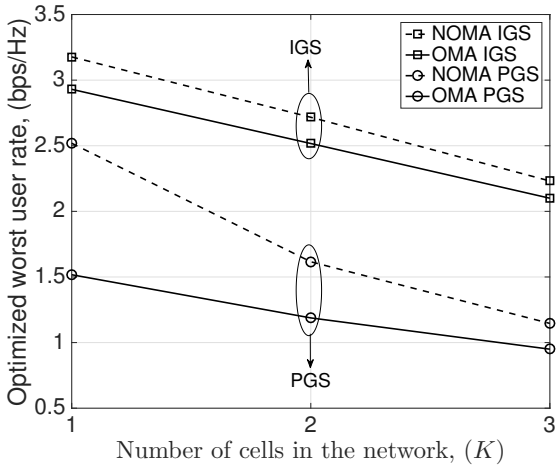

Fig. 10. Optimized worst user rate for varying number of cells K in the network and fixed $N_t = 3$ BS antennas, $N = 4$ UEs, $P^{\max} = 26$ dBm.

and applying inequality (52) to the first term and inequality (51) to the second term, one obtains

$$\begin{aligned} f(\mathbf{X}_1, \mathbf{X}_2) \quad \geq \\ \ln|\mathbf{I}_2 + [\bar{\mathbf{X}}_1]^2\left([\bar{\mathbf{X}}_2]^2 + \sigma^2\mathbf{I}_2\right)^{-1}| + 4 \\ -\sigma^2\langle\left([\bar{\mathbf{X}}_2]^2 + \sigma^2\mathbf{I}_2\right)^{-1}\rangle \\ -\left\langle\sum_{i=1}^{2}[\bar{\mathbf{X}}_i]^2 + \sigma^2\mathbf{I}_2, \left(\sum_{i=1}^{2}[\mathbf{X}_i]^2 + \sigma^2\mathbf{I}_2\right)^{-1}\right\rangle \qquad (53) \\ -\langle\left([\bar{\mathbf{X}}_2]^2 + \sigma^2\mathbf{I}_2\right)^{-1}, [\mathbf{X}_2]^2 + \sigma^2\mathbf{I}_2\rangle. \qquad (54) \end{aligned}$$

Further, applying the inequality

$$[\mathbf{X}_i]^2 \succeq \mathbf{X}_i\bar{\mathbf{X}}_i^T + \bar{\mathbf{X}}_i\mathbf{X}_i^T - [\bar{\mathbf{X}}_i]^2, \qquad (55)$$

which is an equivalent expression of the obvious inequality $[\mathbf{X}_i - \bar{\mathbf{X}}_i]^2 \succeq 0$, to the term (53) yields

$$\begin{aligned} \left\langle\sum_{i=1}^{2}[\bar{\mathbf{X}}_i]^2 + \sigma^2\mathbf{I}_2, \left(\sum_{i=1}^{2}[\mathbf{X}_i]^2 + \sigma^2\mathbf{I}_2\right)^{-1}\right\rangle \quad \leq \\ \left\langle\sum_{i=1}^{2}[\bar{\mathbf{X}}_i]^2 + \sigma^2\mathbf{I}_2, \langle\left(\sum_{i=1}^{2}\left(\bar{\mathbf{X}}_i\mathbf{X}_i^T + \mathbf{X}_i\bar{\mathbf{X}}_i^T\right.\right.\right. \\ \left.\left.\left. -[\bar{\mathbf{X}}_i]^2\right) + \sigma^2\mathbf{I}_2\right)^{-1}\right\rangle \qquad (56) \end{aligned}$$

over the trust region (27)[4], for which we have also used the inequalities $\langle\mathcal{B}, \mathbf{X}\rangle \geq \langle\mathcal{B}, \bar{\mathbf{X}}\rangle$ for $\mathcal{B} \succeq 0$ and $\mathbf{X} \succeq \bar{\mathbf{X}} \succ 0$, and $0 \prec \mathbf{X}^{-1} \preceq \bar{\mathbf{X}}^{-1}$ for $\mathbf{X} \succeq \bar{\mathbf{X}} \succ 0$. Now, the RHS of (26) is obtained from the RHS of (54) upon replacing the term (53) by the RHS of (56).

[4]Since the left hand side of (55) is positive definite, it is meaningful only under the trust region (27), which constrains the RHS of (55) positive semi-definite.

REFERENCES

[1] I. E. Telatar, "Capacity of multi-antenna Gaussian channels," *Eur. Trans. Telecommun.*, vol. 10, no. 6, pp. 585–595, Nov./Dec. 1999.

[2] P. Viswanath and D. N. C. Tse, "Sum capacity of the vector Gaussian broadcast channel and uplink-downlink duality," *IEEE Trans. Inf. Theory*, vol. 49, no. 8, pp. 1912–1921, Aug. 2003.

[3] S. Vishwanath, N. Jindal, and A. Goldsmith, "Duality, achievable rates, and sum-rate capacity of Gaussian MIMO broadcast channels," *IEEE Trans. Inf. Theory*, vol. 49, no. 10, pp. 2658–2668, Oct. 2003.

[4] G. Caire and S. Shamai, "On the achievable throughput of a multiantenna gaussian broadcast channel," *IEEE Trans. Inf. Theory*, vol. 49, no. 7, pp. 1691–1706, July 2003.

[5] H. Weingarten, Y. Steinberg, and S. S. Shamai, "The capacity region of the gaussian multiple-input multiple-output broadcast channel," *IEEE Trans. Inf. Theory*, vol. 52, no. 9, pp. 3936–3964, Sep. 2006.

[6] C. Hellings and W. Utschick, "On the inseparability of parallel MIMO broadcast channels with linear transceivers," *IEEE Trans. Signal Process.*, vol. 59, no. 12, pp. 6273–6278, Dec. 2011.

[7] Y. Zeng, C. M. Yetis, E. Gunawan, Y. L. Guan, and R. Zhang, "Transmit optimization with improper Gaussian signaling for interference channels," *IEEE Trans. Signal Process.*, vol. 61, no. 11, pp. 2899–2913, Jun. 2013.

[8] Z. K. M. Ho and E. Jorswieck, "Improper Gaussian signaling on the two-user SISO interference channel," *IEEE Trans. Wireless Commun.*, vol. 11, no. 9, pp. 3194–3203, September 2012.

[9] C. Lameiro and I. Santamaría, "Degrees-of-freedom for the 4-user SISO interference channel with improper signaling," in *Proc IEEE International Conference on Communications (ICC)*, June 2013, pp. 3053–3057.

[10] H. D. Nguyen, R. Zhang, and S. Sun, "Improper signaling for symbol error rate minimization in k-user interference channel," *IEEE Trans. Commun.*, vol. 63, no. 3, pp. 857–869, Mar. 2015.

[11] C. Hellings and W. Utschick, "Improper signaling versus time-sharing in the SISO Z-interference channel," *IEEE Communications Letters*, vol. 21, no. 11, pp. 2432–2435, Nov 2017.

[12] E. Kurniawan and S. Sun, "Improper Gaussian signaling scheme for the Z-interference channel," *IEEE Trans. Wireless Commun.*, vol. 14, no. 7, pp. 3912–3923, Jul. 2015.

[13] C. Lameiro, I. Santamaría, and P. J. Schreier, "Rate region boundary of the SISO Z-interference channel with improper signaling," *IEEE Trans. on Commun.*, vol. 65, no. 3, pp. 1022–1034, March 2017.

[14] V. R. Cadambe, S. A. Jafar, and C. Wang, "Interference alignment with asymmetric complex signaling—settling the Host-Madsen-Nosratinia conjecture," *IEEE Trans. Inf. Theory*, vol. 56, no. 9, pp. 4552–4565, Sept 2010.

[15] C. Hellings, M. Joham, and W. Utschick, "QoS feasibility in MIMO broadcast channels with widely linear transceivers," *IEEE Signal Process. Letts.*, vol. 20, no. 11, pp. 1134–1137, Nov. 2013.

[16] S. A. Jafar, "Interference alignment-a new look at signal dimensions in a communication network," *Found. Trends Commun. Inf. Theory*, vol. 7, no. 1, pp. 1–134, 2011. [Online]. Available: http://dx.doi.org/10.1561/0100000047

[17] L. Yang and W. Zhang, "Interference alignment with asymmetric complex signaling on MIMO X channels," *IEEE Trans. Commun.*, vol. 62, no. 10, pp. 3560–3570, Oct 2014.

[18] S. Lagen, A. Agustin, and J. Vidal, "On the superiority of improper Gaussian signaling in wireless interference MIMO scenarios," *IEEE Trans. Commun.*, vol. 64, no. 8, pp. 3350–3368, Aug. 2016.

[19] ——, "Coexisting linear and widely linear transceivers in the MIMO interference channel," *IEEE Trans. Signal Process.*, vol. 64, no. 3, pp. 652–664, Feb 2016.

[20] H. Shin, S. Park, H. Park, and I. Lee, "A new approach of interference alignment through asymmetric complex signaling and multiuser diversity," *IEEE Trans. on Wirel. Commun.*, vol. 11, no. 3, pp. 880–884, March 2012.

[21] Y. Zeng, R. Zhang, E. Gunawan, and Y. L. Guan, "Optimized transmission with improper Gaussian signaling in the k-user MISO interference channel," *IEEE Trans. Wirel. Commun.*, vol. 12, no. 12, pp. 6303–6313, December 2013.

[22] A. H. Phan, H. D. Tuan, H. H. Kha, and D. T. Ngo, "Nonsmooth optimization for efficient beamforming in cognitive radio multicast transmission," vol. 60, no. 6, pp. 2941–2951, Jun. 2012.

[23] A. A. Nasir, H. D. Tuan, D. T. Ngo, T. Q. Duong, and H. V. Poor, "Beamforming design for wireless information and power transfer systems: Receive power-splitting vs transmit time-switching," *IEEE Trans. Commun.*, vol. 65, no. 2, pp. 876–889, 2017.

[24] A. Benjebbour, A. Li, Y. Kishiyama, H. Jiang, and T. Nakamura, "System-level performance of downlink NOMA combined with SU-MIMO for future LTE enhancements," in *Proc. IEEE Globecom Workshops (GC Wkshps)*, Dec. 2014, pp. 706–710.

[25] Z. Ding, R. Schober, and H. V. Poor, "A general MIMO framework for NOMA downlink and uplink transmission based on signal alignment," *IEEE Trans. Wireless Commun.*, vol. 15, no. 6, pp. 4438–4454, June 2016.

[26] Z. Ding, F. Adachi, and H. V. Poor, "The application of MIMO to non-orthogonal multiple access," *IEEE Trans. Wireless Commun.*, vol. 15, no. 1, pp. 537–552, Jan 2016.

[27] Z. Ding, Y. Liu, J. Choi, Q. Sun, M. Elkashlan, C.-L. I, and H. V. Poor, "Application of non-orthogonal multiple access in LTE and 5G networks," *IEEE Commun. Mag.*, vol. 55, no. 2, pp. 185–191, Feb. 2017.

[28] W. Shin, M. Vaezi, B. Lee, D. J. Love, J. Lee, and H. V. Poor, "Non-orthogonal multiple access in multi-cell networks: Theory, performance, and practical challenges," *IEEE Commun. Mag.*, vol. 55, no. 10, pp. 176–183, Oct. 2017.

[29] E. Che, H. D. Tuan, H. H. M. Tam, and H. H. Nguyen, "Successive interference mitigation in multiuser MIMO interference channels," *IEEE Trans. Commun.*, vol. 63, no. 6, pp. 2185–2199, June 2015.

[30] H. H. M. Tam, H. D. Tuan, and D. T. Ngo, "Successive convex quadratic programming for quality-of-service management in full-duplex MU-MIMO multicell networks," *IEEE Trans. Commun.*, vol. 64, no. 6, pp. 2340–2353, June 2016.

[31] H. D. Tuan, H. H. M. Tam, H. H. Nguyen, T. Q. Duong, and H. V. Poor, "Superposition signaling in broadcast interference networks," *IEEE Trans. Commun.*, vol. 65, no. 11, pp. 4646–4656, Nov. 2017.

[32] V. D. Nguyen, H. D. Tuan, T. Q. Duong, H. V. Poor, and O. S. Shin, "Precoder design for signal superposition in MIMO-NOMA multicell networks," *IEEE J. Select. Areas Commun.*, vol. 35, no. 12, pp. 2681–2695, Dec 2017.

[33] P. Gahinet and P. Apkarian, "A linear matrix inequality approach to H_∞ control," *Int. J. Nonlinear Robust Control*, vol. 4, pp. 421–448, 1994.

[34] P. Apkarian and H. D. Tuan, "Concave programming in control theory," *J. of Global Optimization*, vol. 15, pp. 343–370, 1999.

[35] Y. Shi, H. D. Tuan, and P. Apkarian, "Nonconvex spectral optimization algorithms for reduced-order $\mathcal{H}_\infty$ LPV-LFT controllers," *Int. J. Nonlinear Robust Control*, vol. 27, pp. 4421–4442, 2017.

[36] D. Peaucelle, D. Henrion, and Y. Labit, "Users guide for SeDuMi interface 1.04," 2002. [Online]. Available: http://homepages.laas.fr/peaucell/software/sdmguide.pdf

[37] E. Bjornson and E. Jorswieck, *Optimal Resource Allocation in Coordinated Multi-cell Systems*. Now Publishers, 2013.

[38] S. Christensen, R. Agarwal, E. Carvalho, and J. Cioffi, "Weighted sum-rate maximization using weighted MMSE for MIMO-BC beamforming design," *IEEE Trans. Wireless Commun.*, vol. 7, no. 12, pp. 4792–4799, Dec. 2008.

[39] H. Tuy, *Convex Analysis and Global Optimization (second edition)*. Springer International, 2016.

[40] R. A. Horn and C. R. Johnson, *Matrix analysis (second edition)*. Cambridge University Press, 1985.

[41] U. Rashid, H. D. Tuan, H. H. Kha, and H. H. Nguyen, "Joint optimization of source precoding and relay beamforming in wireless MIMO relay networks," *IEEE Trans. Commun.*, vol. 62, no. 2, pp. 488–499, Feb. 2014.

[42] S. Sun, T. S. Rappaport, S. Rangan, T. A. Thomas, A. Ghosh, I. Z. Kovacs, I. Rodriguez, O. Koymen, A. Partyka, and J. Jarvelainen, "Propagation path loss models for 5G urban micro- and macro-cellular scenarios," in *Proc. IEEE Vehicular Technology Conference (VTC Spring)*, May 2016, pp. 1–6.

Hoang Duong Tuan received the Diploma (Hons.) and Ph.D. degrees in applied mathematics from Odessa State University, Ukraine, in 1987 and 1991, respectively. He spent nine academic years in Japan as an Assistant Professor in the Department of Electronic-Mechanical Engineering, Nagoya University, from 1994 to 1999, and then as an Associate Professor in the Department of Electrical and Computer Engineering, Toyota Technological Institute, Nagoya, from 1999 to 2003. He was a Professor with the School of Electrical Engineering and Telecommunications, University of New South Wales, from 2003 to 2011. He is currently a Professor with the School of Electrical and Data Engineering, University of Technology Sydney. He has been involved in research with the areas of optimization, control, signal processing, wireless communication, and biomedical engineering for more than 20 years.

Ali Arshad Nasir (S'09-M'13) is an Assistant Professor in the Department of Electrical Engineering, King Fahd University of Petroleum and Minerals (KFUPM), Dhahran, KSA. Previously, he held the position of Assistant Professor in the School of Electrical Engineering and Computer Science (SEECS) at National University of Sciences & Technology (NUST), Paksitan, from 2015-2016. He received his Ph.D. in telecommunications engineering from the Australian National University (ANU), Australia in 2013 and worked there as a Research Fellow from 2012-2015. His research interests are in the area of signal processing in wireless communication systems. He is an Associate Editor for IEEE Canadian Journal of Electrical and Computer Engineering.

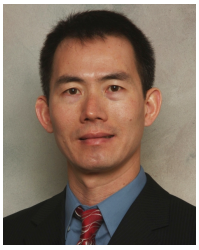

Ha H. Nguyen (M'01, SM'05) received the B.Eng. degree from Hanoi University of Technology (HUT), Hanoi, Vietnam, in 1995, the M.Eng. degree from the Asian Institute of Technology (AIT), Bangkok, Thailand, in 1997, and the Ph.D. degree from the University of Manitoba, Winnipeg, MB, Canada, in 2001, all in electrical engineering. He joined the Department of Electrical and Computer Engineering, University of Saskatchewan, Saskatoon, SK, Canada, in 2001, and became a full Professor in 2007. He currently holds the position of NSERC/Cisco Industrial Research Chair in Low-Power Wireless Access for Sensor Networks. His research interests fall into broad areas of Communication Theory, Wireless Communications, and Statistical Signal Processing. Dr. Nguyen was an Associate Editor for the IEEE Transactions on Wireless Communications and IEEE Wireless Communications Letters during 2007-2011 and 2011-2016, respectively. He currently serves as an Associate Editor for the IEEE Transactions on Vehicular Technology. He was a Co-chair for the Multiple Antenna Systems and Space-Time Processing Track, IEEE Vehicular Technology Conferences (Fall 2010, Ottawa, ON, Canada and Fall 2012, Quebec, QC, Canada), Lead Co-chair for the Wireless Access Track, IEEE Vehicular Technology Conferences (Fall 2014, Vancouver, BC, Canada), Lead Co-chair and Co-chair for the Multiple Antenna Systems and Cooperative Communications Track, IEEE Vehicular Technology Conference (Fall 2016, Montreal, QC, Canada and Spring 2018, Porto, Portugal), and Technical Program Co-chair for Canadian Workshop on Information Theory (2015, St. John's, NL, Canada). He is a coauthor, with Ed Shwedyk, of the textbook "A First Course in Digital Communications" (published by Cambridge University Press). Dr. Nguyen is a Fellow of the Engineering Institute of Canada (EIC) and a Registered Member of the Association of Professional Engineers and Geoscientists of Saskatchewan (APEGS).

Trung Q. Duong (S'05, M'12, SM'13) received his Ph.D. degree in Telecommunications Systems from Blekinge Institute of Technology (BTH), Sweden in 2012. Currently, he is with Queen's University Belfast (UK), where he was a Lecturer (Assistant Professor) from 2013 to 2017 and a Reader (Associate Professor) from 2018. His current research interests include Internet of Things (IoT), wireless communications, molecular communications, and signal processing. He is the author or co-author of 300+ technical papers published in scientific journals (190 articles) and presented at international conferences (132 papers).

Dr. Duong currently serves as an Editor for the IEEE TRANSACTIONS ON WIRELESS COMMUNICATIONS, IEEE TRANSACTIONS ON COMMUNICATIONS, IET COMMUNICATIONS, and a Lead Senior Editor for IEEE COMMUNICATIONS LETTERS. He was awarded the Best Paper Award at the IEEE Vehicular Technology Conference (VTC-Spring) in 2013, IEEE International Conference on Communications (ICC) 2014, IEEE Global Communications Conference (GLOBECOM) 2016, and IEEE Digital Signal Processing Conference (DSP) 2017. He is the recipient of prestigious Royal Academy of Engineering Research Fellowship (2016-2021) and has won a prestigious Newton Prize 2017.

H. Vincent Poor (S'72, M'77, SM'82, F'87) received the Ph.D. degree in EECS from Princeton University in 1977. From 1977 until 1990, he was on the faculty of the University of Illinois at Urbana-Champaign. Since 1990 he has been on the faculty at Princeton, where he is currently the Michael Henry Strater University Professor of Electrical Engineering. During 2006 to 2016, he served as Dean of Princeton's School of Engineering and Applied Science. He has also held visiting appointments at several other universities, including most recently at Berkeley and Cambridge. His research interests are in the areas of information theory and signal processing, and their applications in wireless networks, energy systems and related fields. Among his publications in these areas is the recent book *Information Theoretic Security and Privacy of Information Systems* (Cambridge University Press, 2017).

Dr. Poor is a member of the National Academy of Engineering and the National Academy of Sciences, and is a foreign member of the Chinese Academy of Sciences, the Royal Society, and other national and international academies. He received the Marconi and Armstrong Awards of the IEEE Communications Society in 2007 and 2009, respectively. Recent recognition of his work includes the 2017 IEEE Alexander Graham Bell Medal, Honorary Professorships at Peking University and Tsinghua University, both conferred in 2017, and a D.Sc. *honoris causa* from Syracuse University also awarded in 2017.